Journal of Computational Neuroscience, 2, 215–235 (1995)

Modeling the Leech Heartbeat Elemental Oscillator I. Interactions of Intrinsic and Synaptic Currents

FARZAN NADIM
Department of Biology, Emory University, 1510 Clifton Rd., Atlanta, GA 30322
fnadim@biology.emory.edu

ØYSTEIN H. OLSEN
Department of Biology, Emory University, 1510 Clifton Rd., Atlanta, GA 30322
oolsen@biology.emory.edu

ERIK DE SCHUTTER
The Born Bunge Foundation, University of Antwerp, B2610 Antwerp, Belgium
erikds@reks.uia.ac.be

RONALD L. CALABRESE
Department of Biology, Emory University, 1510 Clifton Rd., Atlanta, GA 30322
rcalabre@biology.emory.edu

Received December 7, 1994; Revised March 9, 1995; Accepted (in revised form) March 17, 1995

Action Editor: T. Williams

Abstract. We have developed a biophysical model of a pair of reciprocally inhibitory interneurons comprising an elemental heartbeat oscillator of the leech. We incorporate various intrinsic and synaptic ionic currents based on voltage-clamp data. Synaptic transmission between the interneurons consists of both a graded and a spike-mediated component. By using maximal conductances as parameters, we have constructed a canonical model whose activity appears close to the real neurons. Oscillations in the model arise from interactions between synaptic and intrinsic currents. The inhibitory synaptic currents hyperpolarize the cell, resulting in activation of a hyperpolarization-activated inward current I_h and the removal of inactivation from regenerative inward currents. These inward currents depolarize the cell to produce spiking and inhibit the opposite cell. Spike-mediated IPSPs in the inhibited neuron cause inactivation of low-threshold Ca^{++} currents that are responsible for generating the graded synaptic inhibition in the opposite cell. Thus, although the model cells can potentially generate large graded IPSPs, synaptic inhibition during canonical oscillations is dominated by the spike-mediated component.

Keywords: central pattern generator, half-center oscillator

Introduction

In many organisms the rhythmic motor activity underlying behavior such as swimming, feeding and heartbeat is controlled by small neuronal networks that include pairs or groups of neurons connected via reciprocally inhibitory synapses (Arshavsky et al., 1993; Calabrese and De Schutter 1992; Friesen, 1989; Satterlie, 1985; Selverston and Moulins, 1985). Interactions among such reciprocally inhibitory neurons often gives rise to rhythmic motor patterns, even when the individual neurons are not oscillatory. Oscillations in such a network depend crucially on interactions among the synaptic and voltage-gated intrinsic currents. A network of reciprocally inhibitory neurons that permits detailed experimental analysis is of great value in identifying currents involved in producing oscillations. However, since it is difficult to study the interactions of these currents in the real neurons, a detailed and realistic model based on experimental measurements can guide experimental analysis and promote understanding of

the mechanisms involved in generating the rhythmic patterns.

The circulatory system of the leech *Hirudo medicinalis* includes a pair of bilateral longitudinal blood vessels with muscular walls. The constrictions of these vessels are controlled and coordinated by a set of 17 pairs of segmental heart motor neurons (HE cells) located in the segmental ganglia (3 to 18) of the nerve cord. A network of seven pairs of bilateral segmental heart interneurons (HN cells), located pairwise in the anterior seven ganglia, Fig. 1A1), in turn, provide rhythmic inhibition to the heart motor neurons (Calabrese and Peterson, 1983). Of these seven pairs of interneurons the anterior-most four pairs (HN(1) through HN(4)) are responsible for generating the beat timing in the network (Fig. 1A2) (Calabrese and Peterson, 1983). Each of the bilateral pairs of interneurons HN(3) and HN(4) form inhibitory synaptic connections across the ganglionic midline. These reciprocally inhibitory connections enable the pair to oscillate in bursts of action potentials with a period of 8 to 12 s. The oscillations persist even when the respective ganglion is isolated from the nerve cord. We refer to these pairs of interneurons as the *elemental oscillators*. Interneurons HN(1) and HN(2) make inhibitory synaptic connections with the ipsilateral cells HN(3) and HN(4), but not among themselves (Fig. 1A1). These interneurons serve to coordinate the rhythm and period of the oscillations of cells HN(3) and HN(4). These four pairs of interneurons constitute the *heartbeat timing oscillator* (Calabrese and Peterson, 1983), within the network of heart interneurons. The neuronal oscillation in an isolated elemental oscillator is not significantly different from the oscillation in the intact network (Peterson, 1983a,b). Interneurons HN(5), HN(6), and HN(7) are responsible for coordinating rhythmic input to the motor neurons and do not take part in generating beat oscillations. We have developed a model of an elemental heartbeat oscillator of based on Hodgkin-Huxley dynamics, from data gathered in voltage-clamp experiments identifying various ionic currents in these cells. The model was constructed and tuned to reproduce both passive and active properties of the pair of neurons.

Several voltage-gated intrinsic and synaptic currents have been identified in the heart interneurons of third and fourth ganglia. The voltage-gated intrinsic currents can be divided into two groups: the inward currents and the outward currents. The inward currents comprise low-threshold Ca^{++} currents, with a rapidly inactivating component I_{CaF} and a slowly inactivating component I_{CaS} (Angstadt and Calabrese, 1991), a persistent Na^+ current I_P (Opdyke and Calabrese, 1994), a hyperpolarization-activated inward current I_h produced by a mixed Na^+/K^+ conductance (Angstadt and Calabrese, 1989) and a postulated fast Na^+ current I_{Na}. The outward currents comprise a slowly inactivating component I_{K_1}, a persistent component I_{K_2}, and a fast transient component I_A (Simon et al., 1992). The synaptic currents are mediated by Cl^-; the inhibitory synaptic transmission between the bilateral pair consists of a graded component I_{SynG} (Angstadt and Calabrese, 1991), as well as a spike-mediated component I_{SynS} (Simon et al., 1994). With the sole exception of I_{Na}, all the intrinsic ionic currents have been measured under voltage-clamp conditions and their voltage dependence has been characterized. We have not been able to voltage-clamp the cells well enough to measure I_{Na}. The equations for I_{Na} were derived from the literature and modified to support action potentials in our model.

We used these experimentally measured intrinsic and synaptic currents of the heart interneurons as building blocks of our model. Each model cell has a single isopotential compartment, and the two cells are identical in their endogenous properties. Our model builds on a previous, less detailed, model described in Calabrese and De Schutter (1992) and De Schutter et al. (1993). The model was tuned by varying only the maximal conductances $\bar{g}_{ion}$ of intrinsic and synaptic currents to choose a set of parameters so that various behaviors of the heart interneurons were reproduced. We refer to the model, together with this set of parameters, as the *canonical model.*

Methods

The simulations were done with Neurolab (Olsen, 1994) and PHASEPLANE (developed by G.B. Ermentrout) software on a Sun SPARCstation LX and on PCs with 486 processors under Linux. The simulations were done using a variable time step method (LSODA in NeuroLab and Gear's method in PHASEPLANE). The ionic currents in the model are given by Hodgkin-Huxley type equations (Hodgkin and Huxley, 1952). The generalized Boltzman-type equations describing the rate functions α and β are of the form given by Beeler and Reuter (1977) (see the appendix).

Experimental data for determining the leak conductance and reversal potential were obtained using single-electrode voltage-clamp and discontinuous

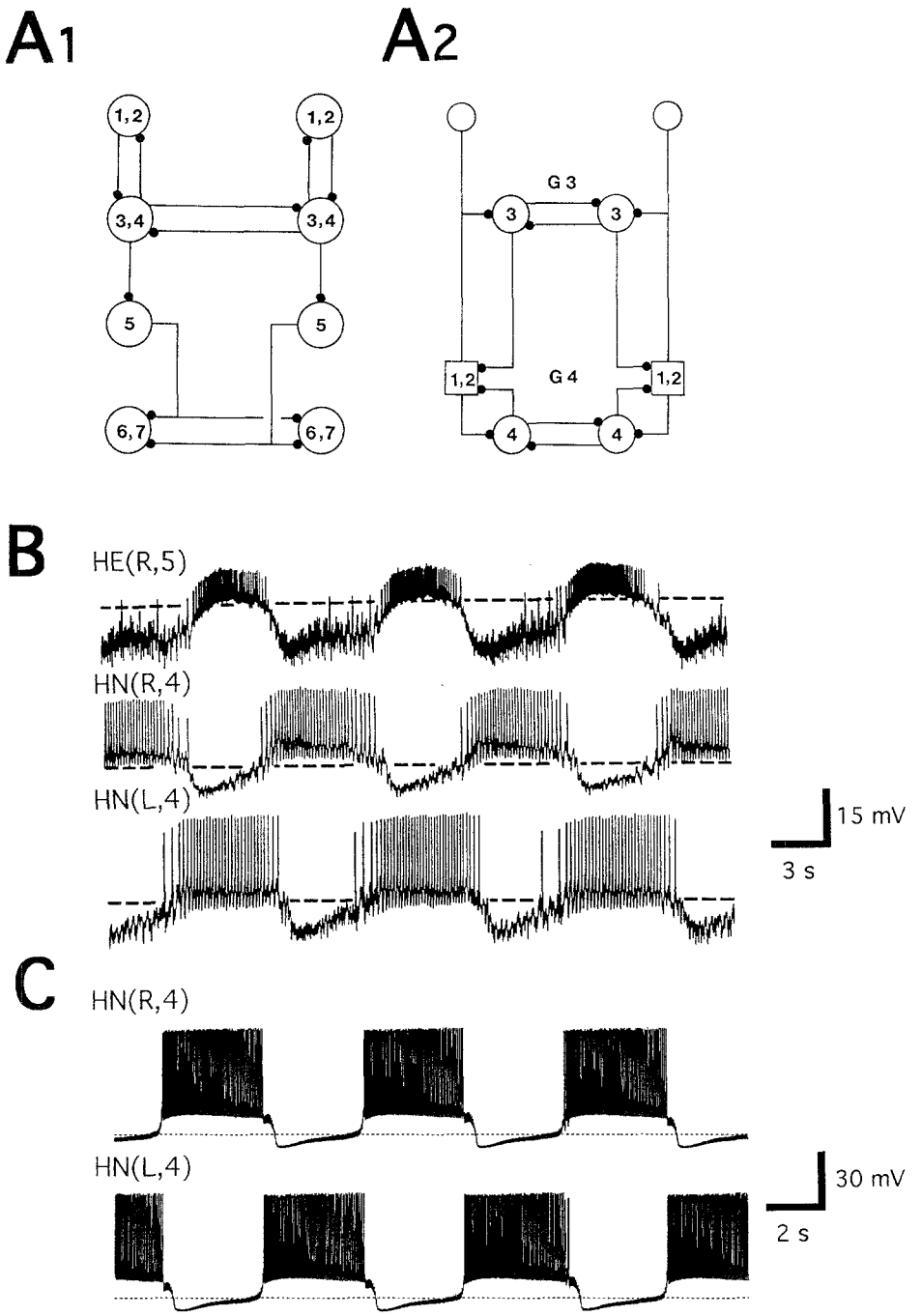

Fig. 1. Synaptic connections and oscillations in the network of leech heart interneurons. A1. The network of seven identified pairs of HN cells responsible for the generation and bilateral coordination of the heartbeat. Cells that have similar connections and oscillate in phase are lumped together. All synaptic connections shown are inhibitory. A2. The heartbeat timing oscillator includes the two elemental oscillators in ganglia 3 and 4. These oscillators are coordinated via inhibitory connections with cells HN(1) and HN(2). B. Oscillations in the elemental oscillator of heart interneurons. Cells HN(R,4) and HN(L,4) oscillate in antiphase. Cell HE(R,5), as well as all ipsilateral heart motor neurons posterior to it, receives inhibition from HN(R,4). Oscillations in heart motor neurons are driven by input from HN cells. The HE(R,5) trace shows large IPSPs during the inhibited phase, partially provided by HN(R,4), and oscillates in antiphase with HN(R,4). Dashed line marks potential of −50 mV. C. Oscillations in the model of the elemental oscillator. Graded and spike-mediated inhibition from each cell to its contralateral homologue and intrinsic properties enable the cells to produce oscillations in antiphase with period of approximately 8 s. The amplitude and frequency of action potentials is larger than in the heart interneurons. Dashed line marks potential of −50 mV.

current-clamp techniques. These experiments were done in leech saline (containing in mMol: NaCl, 115; KCl, 4; $CaCl_2$, 1.8; glucose, 10; and HEPES buffer, 10; adjusted to pH 7.4) with bicuculline methiodide (0.1 mMol) added to block synaptic transmission (Schmidt and Calabrese, 1992) and CsCl (4 mMol) added to block I_h (Angstadt and Calabrese, 1989). Recordings of slow oscillations were obtained in leech saline with elevated Ca^{++} concentration (5 mMol $CaCl_2$) and 10% Na^+ (Na^+ replaced with equimolar *N*-methyl-D-glucamine) and are similar to those described by Arbas and Calabrese (1987).

The interactions and balance of ionic currents that are the building blocks of a conductance-based model, such as the one described here, ultimately determine its output. In constructing such building blocks, we used voltage-clamp measurements of ionic currents in leech heart interneurons. Even though most measurements were fit to data obtained from single cells, we augmented these fits with data obtained from other experiments. The rate equations for I_{CaF} and I_{CaS} were obtained by fitting data from Angstadt and Calabrese (1991); the saturation level of 6 s was chosen for the inactivation time constant of I_{CaS} using long time-step traces of Fig. 6; the deinactivation time constants of I_{CaF} and I_{CaS} was chosen to saturate to approximately 350 ms and 200 ms, respectively (Fig. 9); the steady-state activation and inactivation curves were fit to data from Figs. 3 and 9 and the rate equations were completed by fitting voltage-clamp traces from Fig. 3. The traces were fit with the assumption that conductance values close to the maximal conductances of the (inactivating currents) I_{CaF} and I_{CaS} are obtained. The best fits with these assumptions were obtained with m^2 kinetics. The rate equations for I_h were slightly modified from De Schutter, Angstadt and Calabrese (1993) to fit the range of time constants given in Fig. 4 of Angstadt and Calabrese (1989). The rate equations for I_P were fit to the IV-curve described in Opdyke and Calabrese (1994) (in normal saline). The equations for I_{K_1}, I_{K_2} and I_A were obtained from Simon et al. (1992). The equations for I_{Na} were obtained from literature (Connor and Stevens, 1971; De Schutter, 1986) and modified to produce spiking during bursting oscillations and when synaptic transmission is blocked.

Synaptic transfer between heart interneurons in the third and fourth ganglia includes a graded, as well as a spike-mediated component (Arbas and Calabrese, 1987). With a few minor modifications, our model of the graded component of the synaptic current is as described in De Schutter et al. (1993). The graded synaptic current is dependent on a proportion of the presynaptic concentration of Ca^{++} ([P])

$$I_{SynG} = \bar{g}_{SynG} \frac{[P]^3}{C + [P]^3} (V - E_{Syn}) \qquad (1)$$

where C is a constant that was chosen by fitting the graded synaptic currents (see the appendix). The growth of [P] is linearly dependent on the presynaptic Ca^{++} currents, through a voltage-dependent constant A. The removal of [P] is dependent on [P] itself, through a voltage dependent factor B:

$$\frac{d[P]}{dt} = I_{Ca} - B[P] \quad (I \text{ in nA}) \qquad (2)$$

$$I_{Ca} = \begin{cases} -(I_{CaF} + I_{CaS}) - A & \text{if} > 0 \\ 0 & \text{otherwise} \end{cases}$$

In the fall-off from the plateau phase of oscillations the decay of Ca^{++} currents follows the decay of voltage with a time delay corresponding to the deactivation of I_{CaF} and I_{CaS}. We replaced solely voltage-dependent A of De Schutter, Angstadt and Calabrese (1993) by a time- and voltage-dependent variable with time constant similar to that of the Ca^{++} currents to avoid artifacts during rapid transitions in membrane potential. The factor $[P]^3/(C + [P]^3)$ in Eq. (1) replaced $[P]^3$ in De Schutter, Angstadt and Calabrese (1993). The new factor still accommodates the cubic rise, but since it is saturating it does not grow without bounds.

Spike-mediated synaptic transfer between heart interneurons in the third and fourth ganglia is dependent on as yet undescribed presynaptic high-threshold Ca^{++} currents (Simon et al., 1994). We modeled the spike-mediated synaptic current to be directly dependent on the occurrence of presynaptic action potentials. The spike-mediated synaptic current was described by an α function

$$I_{SynS} = \bar{g}_{SynS} (1 - e^{-t/\tau_{rise}}) e^{-t/\tau_{fall}} (V - E_{Syn}) \qquad (3)$$

as measured in Simon et al. (1994), where $\tau_{rise} = 2.5$ ms and $\tau_{fall} = 11$ ms are, respectively, the rising and falling time constants of the postsynaptic current.

The synaptic equilibrium potential $E_{Syn} = -62.5$ mV and the I_h equilibrium potential $E_h = -21$ mV were estimated from data in Angstadt and Calabrese (1991) and Angstadt and Calabrese (1989). The equilibrium potentials $E_K = -80$ mV, $E_{Ca} = 135$ mV, and $E_{Na} = 45$ mV have not been directly measured and were estimated to fit voltage-clamp data in Simon et al. (1992) and Angstadt and Calabrese (1991). We

determined the value $E_l = -52.5$ mV using criteria described in the results section. With the exception of E_l, all equilibrium potentials were kept fixed while searching for a canonical model.

Results

In constructing a "canonical" model we endeavored to replicate several features of the heart interneurons. The model cells reproduced ionic currents under voltage-clamp conditions. The time constants of activation and inactivation of the model ionic currents were similar to measured time constants. The model cells produced action potentials during oscillations and when synaptic transmission was blocked. The response of the model cells to a hyperpolarizing step pulse in the absence of I_h was passive with input resistance within the measured biological range. The period of oscillations was within the range of periods observed, that is, at least 8 s, and during the inhibited phase the model cells did not hyperpolarize beyond -60 mV. The spike frequency was close to the range observed (10 Hz). The model cells were capable of producing slow oscillations when external Na^+ was reduced.

We built the single-compartmental model of HN cells assuming the cells are electrotonically compact. Using measurements of time constants from current injections we estimated of the electrotonic length of HN cells to be 1.25 ± 0.42 (mean $\pm$ SD; $n = 16$). The rate equations and equilibrium potentials of all currents (except E_l) were obtained using data from voltage-clamp experiments as described in the methods section and were kept fixed, once determined. The maximal conductances $\bar{g}_{\text{ion}}$ were varied to obtain a model that reproduced the behavior of the heart interneurons closely and could be used for further parameter testing.

Angstadt and Calabrese (1991) have shown that graded synaptic transfer in heart interneurons is correlated with presynaptic Ca^{++}. We followed De Schutter et al. (1993) and modeled the graded synaptic currents to be dependent on the "effective" presynaptic concentrations of Ca^{++} ([P]). By the *effective* concentration of Ca^{++} we mean the portion of the total concentration that is responsible for transmitter release. The dependence on [P] was slightly modified from the model described in De Schutter et al. (1993) (see the methods section) so that the graded synaptic conductance g_{SynG} is a saturating function of [P]. Arbas and Calabrese (1987) had shown that the heart interneurons produce (slow) oscillations in saline with elevated Ca^{++} and reduced Na^+ concentrations. We reproduced such oscillations in the heart interneurons in 10% Na^+ saline containing 5 mMol Ca^{++}. To reproduce similar oscillations in the model cells the maximal conductance $\bar{g}_{\text{SynG}}$ of the graded synaptic current had to be increased (to 300 nS) from the value corresponding to the voltage-clamp data (20 to 30 nS), (Angstadt and Calabrese, 1991)). Spike-mediated synaptic transmission was added in the simplest form possible (see the methods section) as an inhibitory ionic current dependent on the occurrence of an action potential in the opposite cell. The maximal conductance $\bar{g}_{\text{SynS}}$ of the spike-mediated synaptic current was adjusted from the measured value of 12 nS (Simon et al., 1994) to 40 nS so that the amplitude of the spike-mediated IPSPs were 1 to 3 mV (IPSPs observed in the heart interneurons are 1 to 5 mV).

The values of E_l and g_l were determined not just from the data presented in this section but also from the behavior of the model neurons when synaptic transmission was blocked. We also tested the response of an isolated model cell to a hyperpolarizing current pulse when I_h is blocked ($\bar{g}_h = 0$). In response to a hyperpolarizing current step, in addition to the passive response, the model cell showed a delayed hyperpolarization and a sharp drop in membrane potential, consistent with slow deactivation of inward currents. This slow deactivation has not been observed in the heart interneurons and was eliminated in the model cells by making the deactivation rate of I_{P} fast and I_{CaF} and I_{CaS} small at those potentials. Deactivation at these more negative potentials could not be measured accurately in the voltage-clamp studies.

The threshold for activation of the fast Na^+ current I_{Na}, as well as its maximal conductance, was adjusted to insure that the model cells spike when synaptic transmission is blocked, as well as on plateaus produced during oscillations. The spike frequency in the model in these two cases varies through a wider range than it does in the heart interneurons: in the canonical model the spike frequency is 15 to 23 Hz during oscillations Olsen et al. (1995) and approximately 3.5 Hz when synaptic transmission is blocked. These values contrast with 10 Hz and 7.5 Hz, respectively, measured for the heart interneurons. We tried adjusting the spike frequency in the model by varying the maximal conductance of I_A, but because I_A inactivates at relatively negative potentials (Fig. 2) it had a small effect on spike frequency during the bursting oscillations. We adjusted the spike frequency somewhat by varying the maximal conductances of I_{K_1} and I_{K_2}.

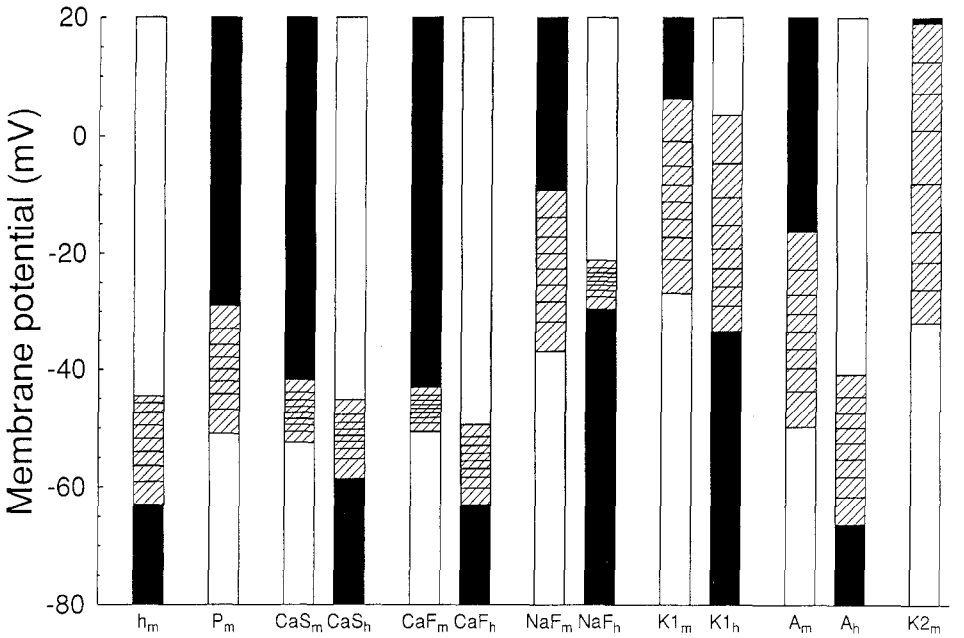

Fig. 2. Steady-state activation and inactivation curves of all voltage-gated intrinsic ionic currents. Black denotes >90% and white denotes <10%. Each mark in the shaded region denotes a 10% change. I_h activates at hyperpolarized potentials but fully activates only at potentials below −70 mV. I_P which has a low activation threshold and a shallow activation curve is partially responsible for supporting plateau formation during the bursting phase of oscillations. Plateau formation is also supported by I_{CaF} and I_{CaS}, which also have low activation thresholds but low inactivation thresholds as well. Ionic currents I_{Na} and I_{K_1} that support action potentials activate at more depolarized potentials than currents that support plateau formation.

Oscillations Arise Through Interactions of Intrinsic and Synaptic Currents

The oscillation of the model cells consisted of two distinct phases: the inhibited phase and the depolarized plateau or the burst phase (Figs. 3 and 4). During the initial part of the inhibited phase, the inhibited cell received both graded and spike-mediated inhibition from the contralateral cell. Graded inhibition, however, waned within the first second and for the remainder of the inhibited phase inhibition was spike-mediated.

During the inhibited phase the cell gradually depolarized until the membrane potential reached the threshold (near −50 mV, the dashed line in Figs. 3 and 4) for plateau formation and burst generation, produced by the regenerative inward currents, I_{CaF}, I_{CaS} and I_P. The depolarization was caused by two factors. First, there was a buildup of inward currents in the postsynaptic cell. The hyperpolarization-activated I_h played a significant role in this build-up and there was a contribution from the leak current (E_l = −52.5 mV). Unlike other ionic currents I_h activates at hyperpolarized potentials and deactivates at depolarized potentials (Figs. 4 and 2). Because I_P has a low activation threshold value and m^1 dynamics, it also helped depolarize the cell during the inhibited phase, even though the main contribution of I_P was during the plateau phase. Second, the synaptic currents decayed. The graded synaptic current did not last for the duration of the inhibitory phase, due both to the inactivation of presynaptic Ca^{++} currents and the removal of the effective Ca^{++} in the presynaptic cell. Because of a decrease in spike frequency, the spike-mediated synaptic current somewhat weakened as well. This decrease was due to a gradual decay of the presynaptic plateau, caused by the inactivation of I_{CaS}, although I_{CaS} never fully inactivated. The threshold of activation of the Ca^{++} currents is around −45 to −50 mV. When this threshold was reached, the regenerative inward currents I_{CaF}, I_{CaS}, and I_P depolarized the cell and initiated the plateau phase that underlies bursting. The inward current I_{CaF} inactivates rapidly, so that it was only active during the rise to the plateau. The plateau was then sustained by I_{CaS} and I_P and was terminated by synaptic currents activated by the contralateral cell when it escaped its inhibited phase. During the plateau phase the cell was

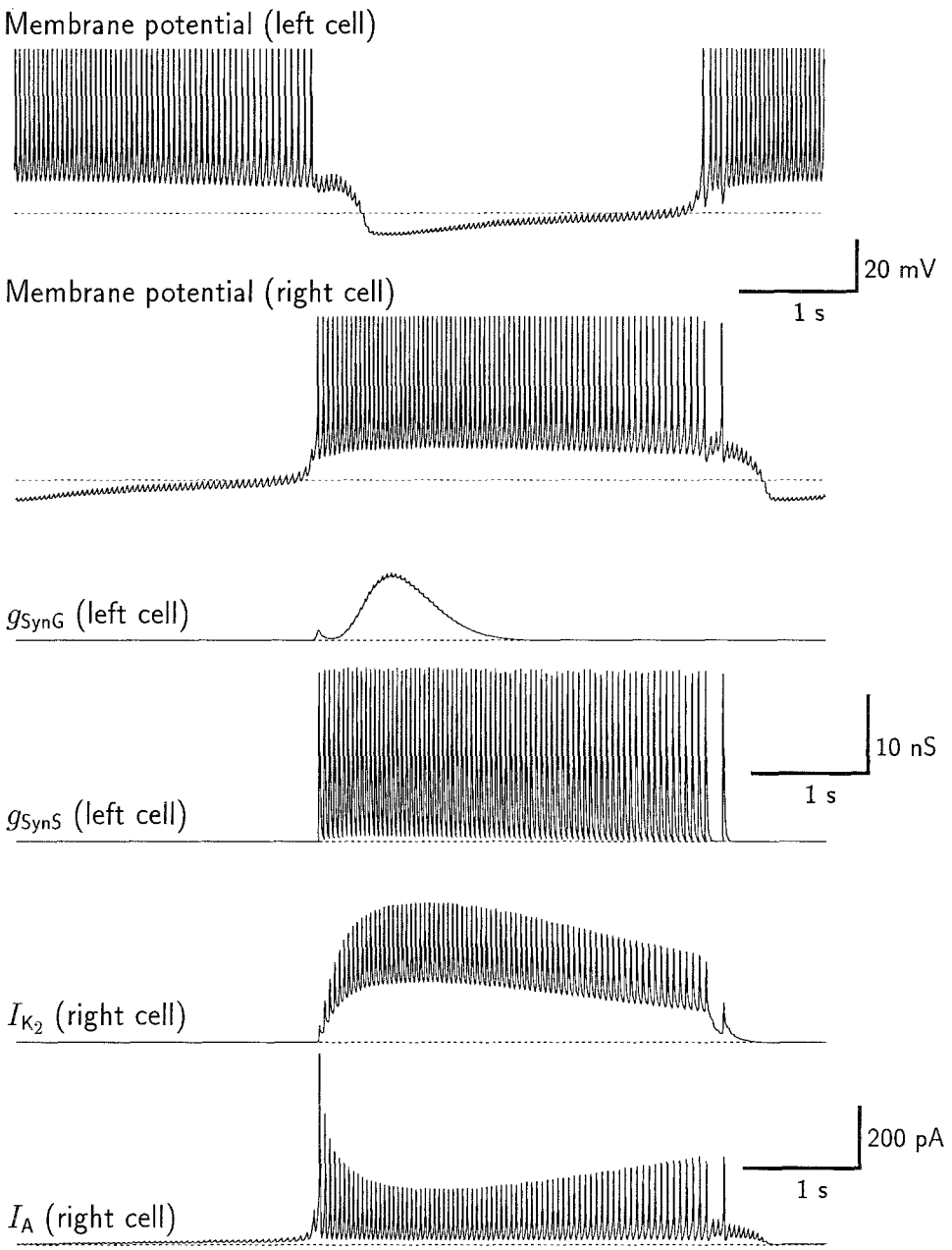

Fig. 3. One cycle of oscillations in the model cells. Synaptic conductances and K^+ currents are shown on the same time scale. g_{SynG} (hence I_{SynG}) was only active during the initial phase of hyperpolarization in the left cell and for the rest of the inhibited phase hyperpolarization was carried by g_{SynS}. I_{K_2} prevented the cell from depolarizing too much during the plateau phase, whereas I_A helped control spiking frequency and slowed down the rise to plateau. The trace for I_{K_1}, which was much larger in size than I_{K_2} and I_A, is not shown.

depolarized to above the threshold for activation of I_{Na}, the rapidly activating and rapidly inactivating inward current responsible for spiking. There was a slight decay in the base potential throughout the plateau due to the slow inactivation of I_{CaS}. The outward currents serve two roles; to regulate the amplitude of plateaus and to regulate spike frequency. Because it is slow to activate and deactivate, and does not inactivate, I_{K_2} is crucial in regulating the amplitude of the plateau; I_{K_2} activated in the burst phase and, together with I_l ($E_l = -52.5$ mV), counteracted the inward currents to prevent the plateau from depolarizing too much.

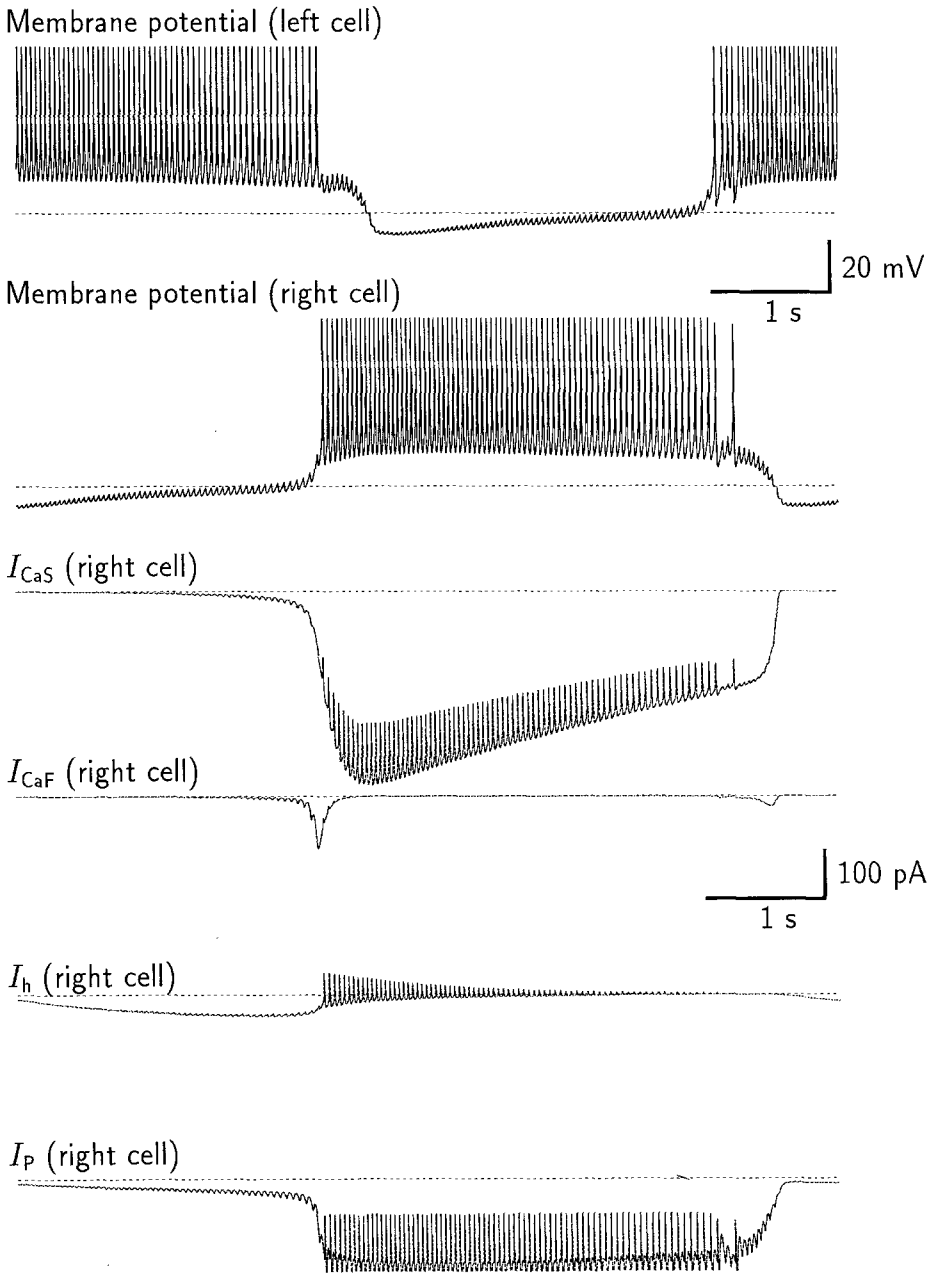

Fig. 4. One cycle of oscillations in the model cells. Inward currents are shown on the same time scale. I_{CaS} and I_P supported the plateau. Inactivation of I_{CaS} resulted in reduction of spiking frequency. I_{CaF} was transient and active only during the beginning and end of the inhibited phase. I_h activated during the inhibited phase and helped depolarize the cell to the threshold of regenerative activation of I_{CaS}, I_{CaF}, and I_P.

A very depolarized plateau could result in inactivation of I_{Na} and cessation of spiking. The outward currents I_{K_1} and I_A affected spike frequency. The falling phase of the action potentials is mainly due to activation of I_{K_1}, although partially due to inactivation of I_{Na} as well.

The Model is Capable of Reproducing Various Passive and Active Properties of the Heart Interneurons

The Passive Response and the Leak Current. From varying the leak conductance g_l and the leak equilibrium potential E_l in the model, we know that the nature

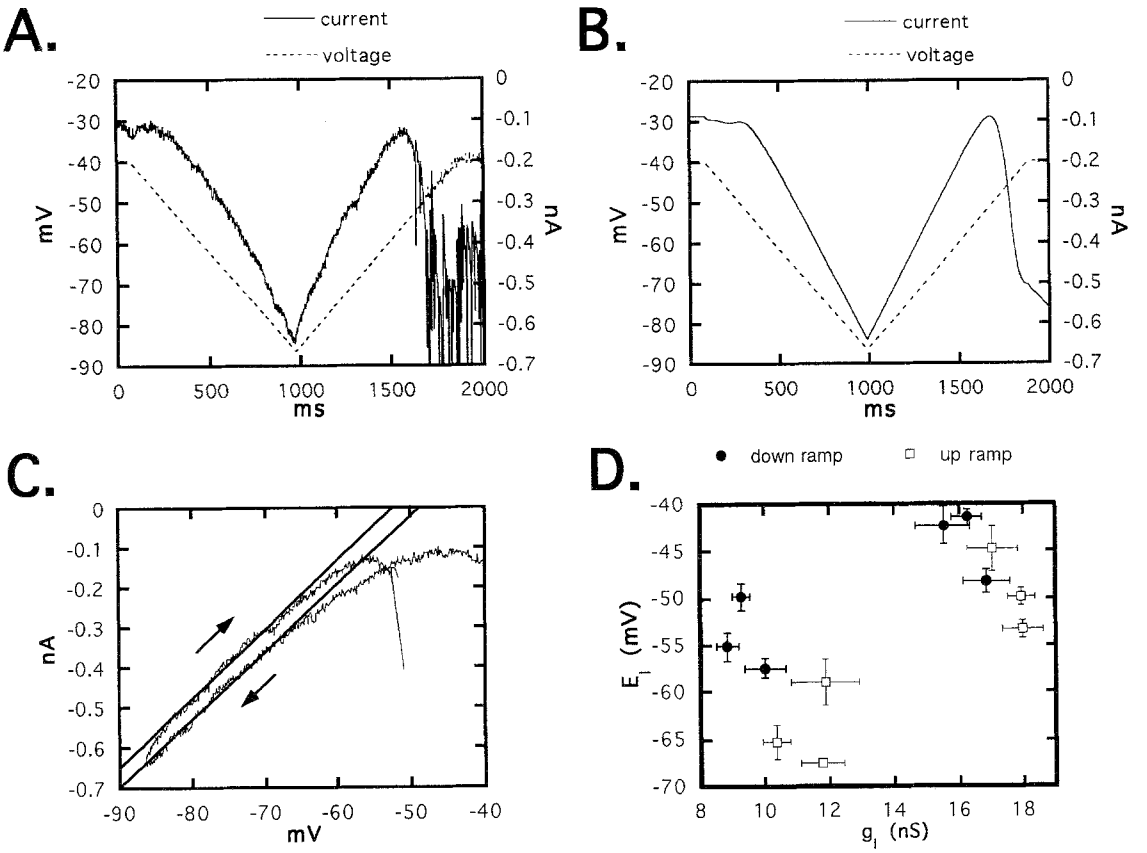

Fig. 5. Measurement of g_l and E_l under voltage-clamp conditions after blocking synaptic transmission (bicuculline 0.1 mMol) and I_h (Cs^+ 4 mMol). A. The cell was voltage-clamped at holding potential of −40 mV. A hyperpolarizing ramp by 45 mV over 1 s followed by a similar depolarizing ramp to the original holding potential was applied and the membrane currents were measured. B. Same protocol used in the model cells. The values g_l and E_l were adjusted to match the values measured in the cell shown in A. C. The IV curve obtained by eliminating time between the voltage and current traces in A. There was a shift in the IV-curve going from the down ramp to the up ramp due to the capacitive current of the cell. D. Values of E_l and g_l measured in 6 cells on the down ramp and the up ramp shown with error bars (mean ± SE, 3 to 9 trials per cell). Lower values of E_l match with lower values of g_l, indicating that cell injury may contribute to the variation.

of oscillations is extremely sensitive to these parameters (Olsen et al., 1995). In practice measuring these parameters is difficult because the measurements of g_l are complicated by activation of voltage-gated currents and the quality of the impalement.

To obtain an estimate of g_l and E_l, without interference from inward currents, we measured the response of the cells to a hyperpolarizing voltage ramp under voltage-clamp conditions ($n = 6$). After blocking synaptic currents (bicuculline 0.1 mMol) and I_h (Cs^+ 4 mMol), the cells were voltage-clamped at holding potentials between −40 and −60 mV. A hyperpolarizing ramp of 45 to 50 mV over 1 s, followed by a similar depolarizing ramp to the original holding potential, was then applied and the membrane currents were measured (Fig. 5A). The IV-curve was plotted and lines were fit to the linear region, both on the down ramp and on the up ramp (Fig. 5C) and E_l estimated by extrapolation to the zero-current axis. Figure 5B shows the response of the model to such a voltage ramp. The current traces on the down ramp in Fig. 5A and B showed a downward inflection which disappears at more negative potentials. The upper portion of the IV-curve in Fig. 5C also shows this downward inflection. These inflections appear to be caused by inward currents (most likely I_P, see below) that deactivate as the cell is hyperpolarized. There was a similar but larger downward inflection at the upper end of the up ramp. This inflection also appeared to be due to the activation of inward currents, and the larger size was probably due to a large contribution from low-threshold Ca^{++} currents that had been deinactivated when the cell was hyperpolarized. The latter part of the current trace in Fig. 5A was contaminated with large fluctuations due to action potentials

that were not voltage-clamped. There was a shift of approximately 50 pA in the current going from the down ramp to the up ramp (Fig. 5C). This shift is due to the capacitive current of the cell, consistent with our estimate of 500 pF. The true value of E_l is the average of the estimated values on the down ramp and the up ramp.

Figure 5D plots the values of E_l versus g_l for six cells (three to nine trials per cell) on both the down ramp and the up ramp. In both cases the cells that had higher g_l, and hence lower input resistance, also had E_l values closer to 0, consistent with the notion that the quality of impalement in these cells affected the values of g_l and E_l. The values of g_l measured (mean ± SE) were 12.8 ± 1.5 nS on the down ramp and 14.5 ± 1.4 nS on the up ramp. The values of E_l measured (mean ± SE) were −48.9 ± 2.7 mV on the down ramp and −56.7 ± 3.6 mV on the up ramp.

From previous measurements of the membrane resistance of the cells, and from data presented here, we used $g_l = 10$ nS as the leak conductance in the model. We then kept g_l fixed and observed the behavior of a single model neuron for different values of E_l (between −65 and −40 mV) when synaptic transmission was blocked ($\bar{g}_{\text{SynS}}$ and $\bar{g}_{\text{SynG}} = 0$). Depending on the value of E_l, the isolated model neuron would be quiescent, tonically spike, show bistability between these two modes, or go through bursting oscillations. The more depolarized values of E_l activated enough inward currents to maintain the model cell above spike threshold and produce tonic spiking, whereas the hyperpolarized values of E_l prevented the activation of inward currents and the model cell was quiescent. Sometimes both responses could be observed (bistability) depending on initial conditions or in response to perturbation with a hyperpolarizing current step. For some intermediate values of E_l (e.g., −57.5 mV) an isolated model cell went through bursting oscillations. The value of $E_l = -52.5$ mV was chosen so that the isolated model cell spikes tonically and, when perturbed by a hyperpolarizing current pulse, has a passive response that is close to the observed response in the heart interneurons.

I_P and the Effect of Blocking Synaptic Transmission. Blocking synaptic transmission between heart interneurons disrupted normal rhythmic activity and caused the cells to fire tonically (Schmidt and Calabrese 1992) (Fig. 6). This effect was mimicked by the model cells when synaptic transmission was removed. The

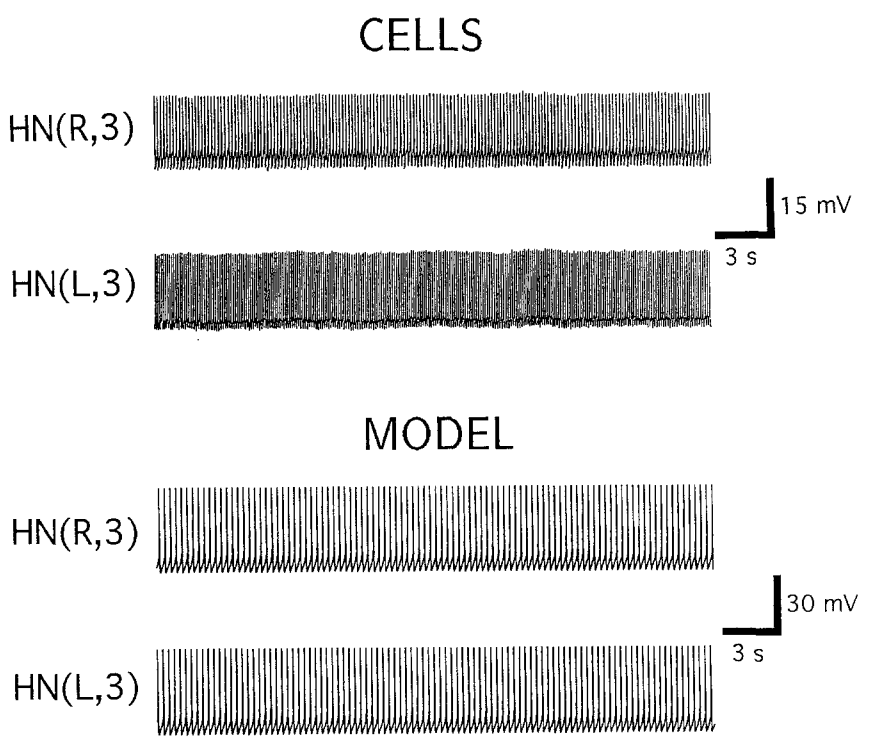

Fig. 6. Effects of blocking synaptic transmission in the elemental oscillator. Application of bicuculline (0.1 mMol) in the bath caused the cells to go into tonic spiking. Oscillations in HN cells are therefore dependent on synaptic interaction between the neurons rather than solely arising from intrinsic properties of the individual neurons. The model cells also fired tonically when synaptic transmission was removed. An analysis of the currents in the model cells revealed that I_P is responsible for maintaining the cells above threshold for spiking.

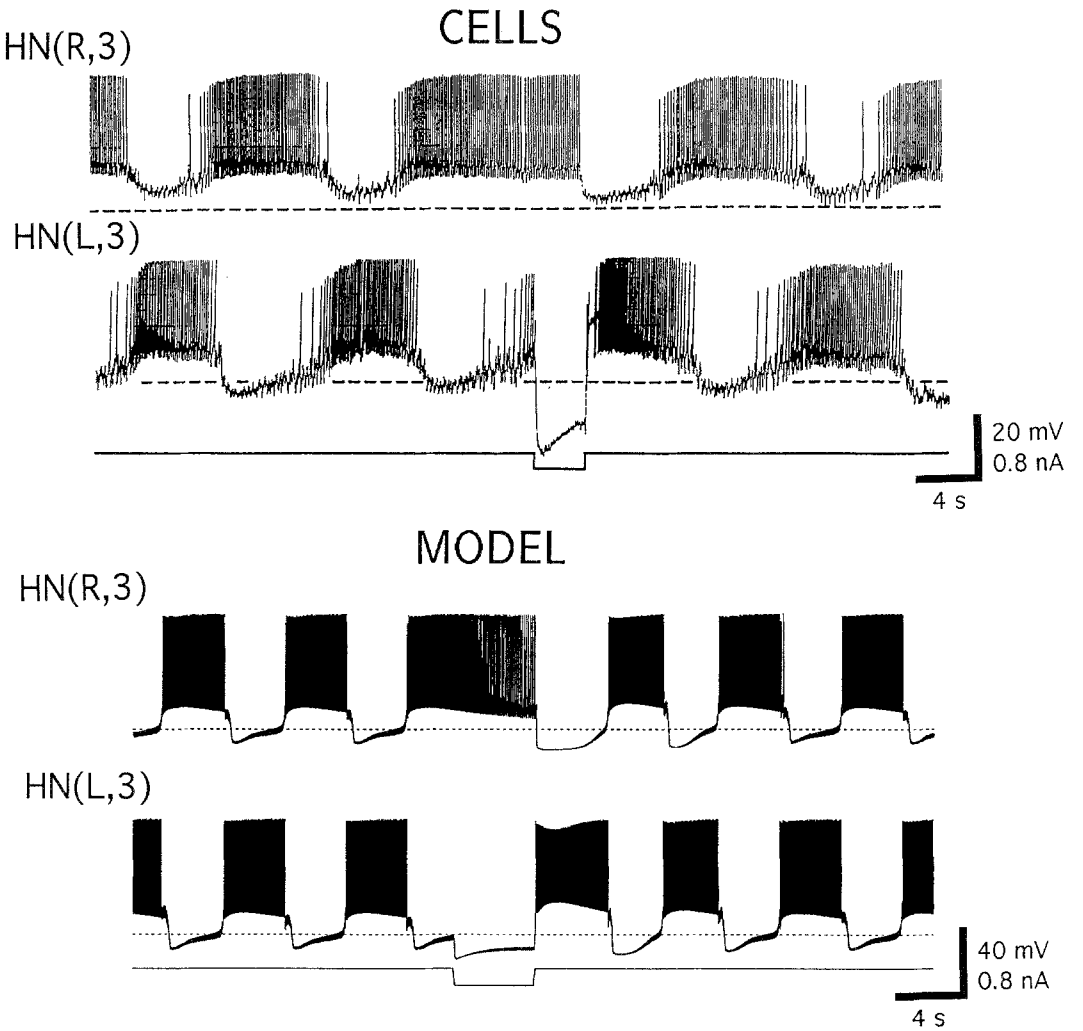

Fig. 7. Hyperpolarizing pulse (−0.2 nA) applied to one neuron in the elemental oscillator. The opposite cell continued spiking for the duration of the pulse and the oscillation was reset on release. During the step the membrane potential of the perturbed cell to "sag" and there was a large plateau on termination of the pulse. Analysis of the ionic currents in the model cells showed that the sag was due to activation of I_h and there was more removal of inactivation ($h_{CaS} = 0.94$ and $h_{CaF} = 0.85$) from I_{CaS} and I_{CaF} than during normal oscillations ($h_{CaS} = 0.83$ and $h_{CaF} = 0.59$). These low-threshold Ca^{++} currents resulted in the large plateau following the pulse.

bottom of the spike undershoots in the model cells was approximately −45 mV. In order to maintain spiking when the oscillations are disrupted, the cells must remain depolarized above the threshold for spiking. Such a depolarizing effect can be obtained either by way of a leak current with sufficiently high equilibrium potential or by inward currents. Our data indicated that E_l is between −55 and −50 mV, (which is below the threshold for spiking) and therefore is incapable of maintaining spiking in the model cells without the help of inward currents. In Fig. 5 we showed that there are inward currents active at −40 mV that deactivate with hyperpolarization. Voltage-clamp measurements in Opdyke and Calabrese (1994) have also shown that I_P has a low threshold for activation and is possibly active at such potentials (Fig. 2). The analysis of ionic currents in the model cells when synaptic transmission was blocked showed that I_P provided the depolarization necessary to maintain the cells above threshold for spiking.

Perturbation Tests in Normal Saline and in 0 Na^+. Figure 7 shows the response of the real and model cells to a hyperpolarizing (−0.2 nA) pulse of current. The effect of such a hyperpolarizing pulse on the oscillations in the heart interneurons was first shown in Arbas and Calabrese (1987). For the duration of the pulse,

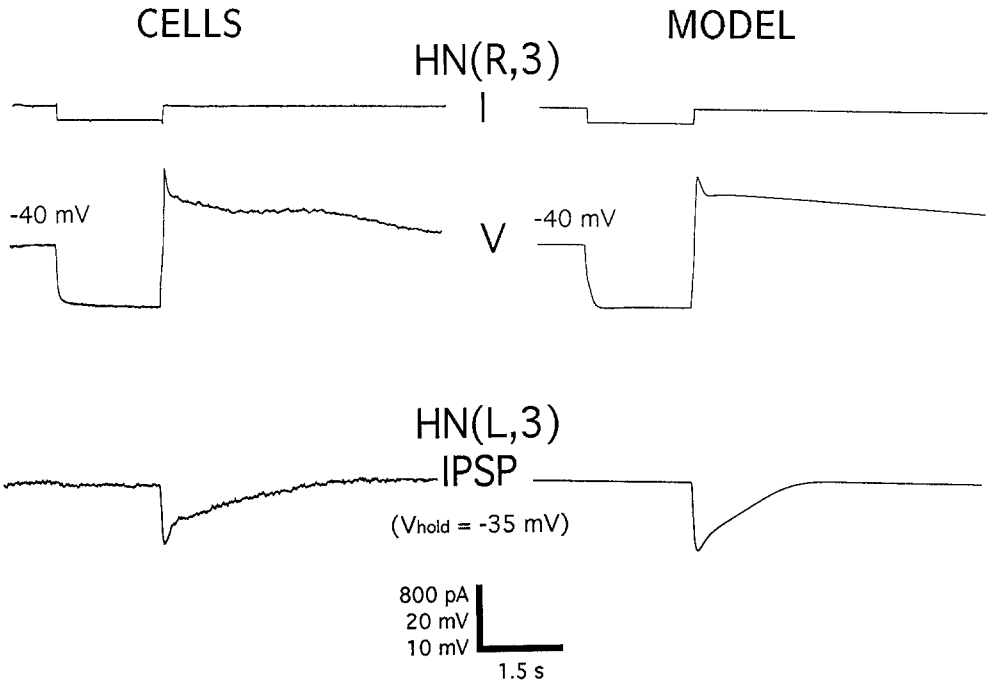

Fig. 8. Hyperpolarizing pulse (−0.2 nA) applied to cell in Na^+-free saline containing 5 mMol Ca^{++} revealed a Ca^{++} plateau and the correlation of the graded IPSP with presynaptic Ca^{++} currents. The plateau consisted of a transient depolarization (due to I_{CaF} in the model cells) as well as a slowly decaying, prolonged depolarization (sustained by I_{CaS} in the model cells). The perturbed cell was held at −40 mV before the pulse was applied. The opposite cell was held at −35 mV to reveal the graded IPSP. The response in model is shown with $\bar{g}_{SynG} = 21$ nS.

the hyperpolarized cell does not escape from the hyperpolarizing current to the burst phase; therefore, the contralateral cell does not receive any synaptic inhibition and continues to spike. In the hyperpolarized cell, a sag potential is seen during the current step. On termination of the pulse, the phase of the oscillation is reset. All these effects were observed in the model cells in response to a hyperpolarizing pulse as well. Analysis of the ionic currents in the model cells during the pulse showed that the sag in the membrane potential of the hyperpolarized cell is due to activation of I_h. Also, during the hyperpolarizing pulse, there was significant removal of inactivation from the low-threshold Ca^{++} currents in the model cell giving rise to large Ca^{++} currents on release from hyperpolarization. The large Ca^{++} currents resulted in a large plateau and a large graded synaptic transmission in the contralateral cell when the pulse was terminated. Similarly in the heart interneurons there was a robust plateau and enhanced graded transmission on release from the hyperpolarizing current pulse (Arbas and Calabrese, 1987).

Injection of a hyperpolarizing current pulse in a quiescent heart interneuron in the absence of Na^+ indicates that low-threshold Ca^{++} currents can support depolarizing plateaus and prolonged graded synaptic transmission (Fig. 8) (Angstadt and Calabrese, 1991). The experiment was done in Na^+-free leech saline with elevated Ca^{++} (5 mMol) and Cs^+ (4 mMol) added to block I_h. A hyperpolarizing pulse was delivered from a holding potential of −40 mV and the cell was hyperpolarized to approximately −60 mV during the current pulse. There was no sag response due to the blocking of I_h. The depolarizing plateau following this pulse consisted of a transient spike-like phase and a prolonged phase at about −30 mV. The contralateral cell (bottom trace) is held at −35 mV to reveal the prolonged synaptic potential associated with the plateau in the perturbed cell. In the model cells the transient phase is due to the rapid activation and inactivation of I_{CaF} and the prolonged phase is due to I_{CaS}.

Slow Oscillations. Figure 9 shows oscillations in the heart interneurons in 10% Na^+ leech saline with elevated Ca^{++} (5 mMol). Reduced Na^+ in the bath prevented the cells from spiking; normal activity was interrupted and the cells were quiescent. Slow oscillations were then triggered by a hyperpolarizing current step in one cell and lasted for approximately 2 minutes. Elevated Ca^{++} in the bath enhanced both the plateaus and the synaptic transfer. The period of

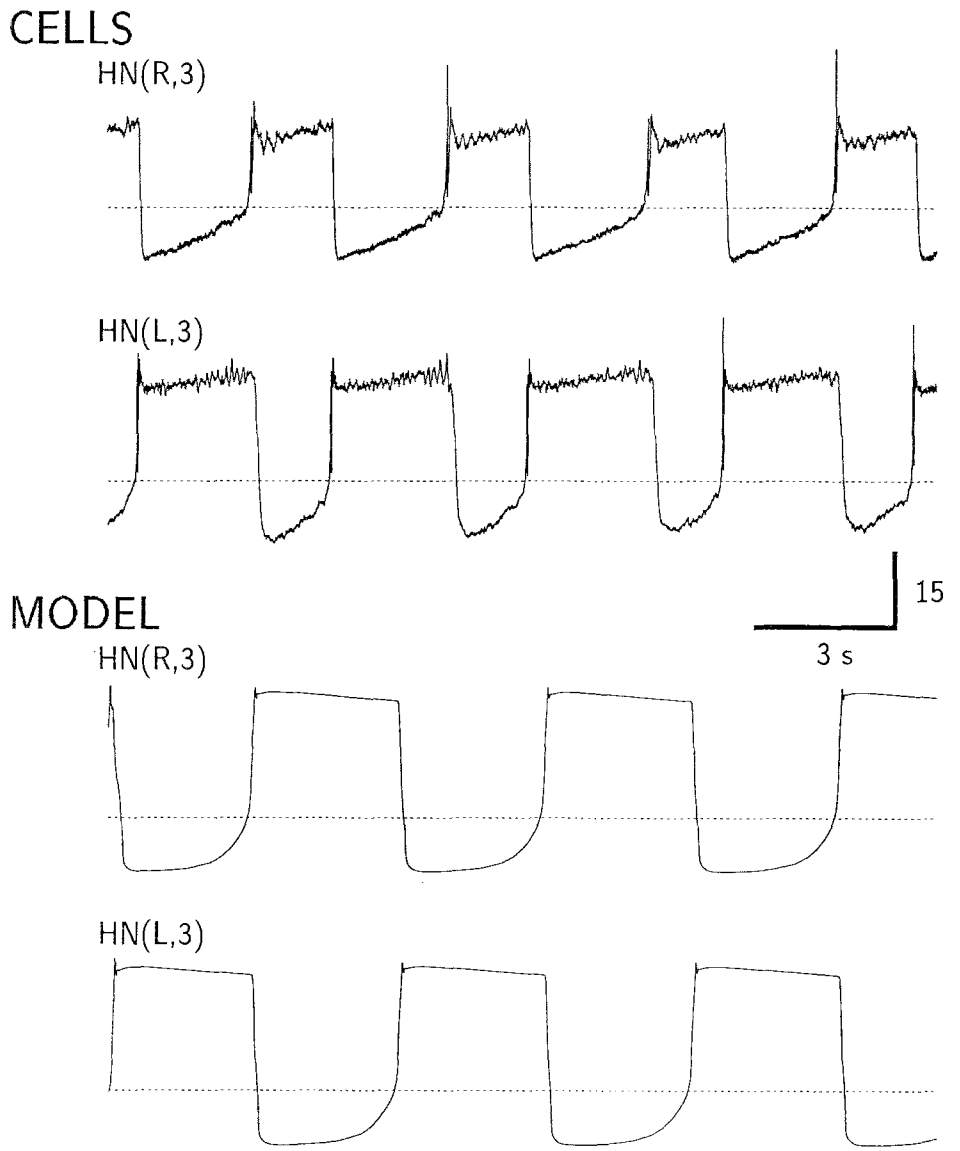

Fig. 9. Slow oscillations of the elemental oscillator in 10% Na^+ saline containing 5 mMol Ca^{++} triggered by a hyperpolarizing pulse (not shown) in one cell. Oscillations are fast and transitions are abrupt. Similar oscillations produced in the model cells by reducing E_{Na} and E_h revealed a large graded IPSP and larger Ca^{++} currents compared to normal oscillations. The slow oscillations are a simple example of G-mode oscillations and show that the interneurons are capable of producing graded IPSPs large enough to sustain oscillatory behavior in the absence of spike-mediated transmission.

oscillations was 4 to 5 s, much faster than the normal period of 8 to 12 s. The transition to plateau was more abrupt making the oscillations relaxation-like and the amplitude of the plateaus was larger than during normal oscillations (Fig. 1). The lower set of traces show slow oscillations in the model cells produced by reducing E_{Na} from 45 mV to -12 mV and E_h from -21 mV to -46 mV, consistent with reducing external Na^+ concentration by 90%. Since action potentials and therefore spike-mediated transfer was eliminated, oscillations in the model cells were maintained solely by graded synaptic transfer. Also, in the model cells, the plateaus were mainly supported by Ca^{++} currents. A comparison of the ionic currents in the model cells during slow oscillations with the normal oscillations (Figs. 3 and 4) revealed a much larger graded IPSP during slow oscillations. Large low-threshold Ca^{++} currents resulted in a large graded IPSP in the opposite

cell. The large graded IPSP (that is, hyperpolarization), in turn, resulted in substantial removal of inactivation from the Ca^{++} currents and hence in large Ca^{++} currents supporting the plateau. Furthermore, during normal oscillations of the model cells, action potentials activated large K^+ currents (mainly I_{K_1}), which subdued the plateaus; the absence of action potentials during slow oscillations resulted in a much more depolarized plateau.

Two Distinct Oscillation Modes

If spike-mediated synaptic transmission was considerably reduced ($\bar{g}_{SynS} < 30$ nS) or blocked ($\bar{g}_{SynS} = 0$), the model cells were still capable of producing oscillations. The synaptic transfer in this case was mainly provided by the graded mechanism (I_{SynG}). The voltage traces from these oscillations were very similar to voltage traces from the first-generation model of the HN elemental oscillator, which contained no specific formulation for spike-mediated transmission (Calabrese and De Schutter, 1992). A comparison of these oscillations with the canonical oscillations of the model cells (when $\bar{g}_{SynS}$ is at its value of 40 nS) revealed a fundamental difference in the balance of intrinsic and synaptic currents between the two modes. In the former mode graded transfer played a dominant role in the oscillations; the graded IPSP lasted for the duration of the inhibited phase and I_{CaS}, I_h, and the amplitude of slow oscillations that underlie bursting were large (Fig. 12). In the latter mode graded synaptic transfer was transient, persisting only for a fraction of the inhibited phase (Fig. 3). Moreover, the cells did not hyperpolarize below −59 mV. We refer to the former oscillations as the *G-mode* and the latter as the *S-mode* (Fig. 10) (Olsen et al., 1995). In Olsen, Nadim and Calabrese (1995) we define these two modes more precisely and show how varying different parameters gives rise to these modes in the model.

G-Mode Oscillations. Bursting in G-mode was marked by oscillations with larger amplitude and shorter period (Figs. 11 and 12). During the inhibited phase, the membrane potential attained values very close to E_{Syn} (−62.5 mV). This large hyperpolarization resulted in considerable removal of inactivation from I_{CaF} and I_{CaS} and in the activation of I_h. The activation of I_h helped the cell depolarize rapidly, and the Ca^{++} currents were regeneratively activated to produce a large plateau on termination of the inhibited phase. The large Ca^{++} currents also resulted in a sizable graded IPSP in the opposite cell (Fig. 11). This large graded IPSP, in turn, caused the opposite cell to hyperpolarize to values close to E_{Syn}, and the cycle repeated.

S-Mode Oscillations. In S-mode, bursting oscillations have a shallower inhibited phase and longer period (Figs. 3 and 4). The regenerative activation of I_{CaS} and I_{CaF} was reduced 25% (peak) by the spike-mediated synaptic transfer in S-mode. The graded IPSP was no longer present during the entirety of the inhibited phase, nor was it as strong. Consequently, the cells did not become so hyperpolarized, there was less removal of inactivation from I_{CaS} and I_{CaF} and less activation of I_h. The smaller Ca^{++} currents resulted in a smaller plateau and a smaller graded IPSP compared to G-mode. When spike-mediated transfer was present, every action potential in the presynaptic cell produced a small IPSC in the postsynaptic cell. The size of this IPSC increased as the postsynaptic cell became more depolarized. By repeatedly tapping down the membrane potential, the spike-mediated IPSCs lengthened the time the cell spent in the −55 to −45 mV range and opposed the regenerative activation of I_{CaF} and I_{CaS}. The increased time spent in this voltage range resulted in considerable inactivation of I_{CaF} and I_{CaS} (both of which are more than 90% inactivated at −45 mV) during the rise to the plateau and, consequently, in a smaller graded IPSP and less activation of I_h in the opposite cell.

Discussion

Is the Model a Faithful Representation of the Heart Interneuron Elemental Oscillator?

The building blocks of the model are intrinsic and synaptic ionic currents that have been measured under voltage-clamp conditions in the heart interneurons (see the introduction). We were not merely interested in building a model that could produce oscillations but in constructing one that would illuminate the mechanisms involved in producing oscillations in the real neurons. We included all described ionic currents in the model, added a fast Na^+ current based on equations from the literature and tuned the maximal conductances to produce a model capable of reproducing or mimicking many of the behaviors of the real neurons. The model builds on a less detailed model described in Calabrese and De Schutter (1992) and De Schutter et al. (1993). The major changes made in the new model were the

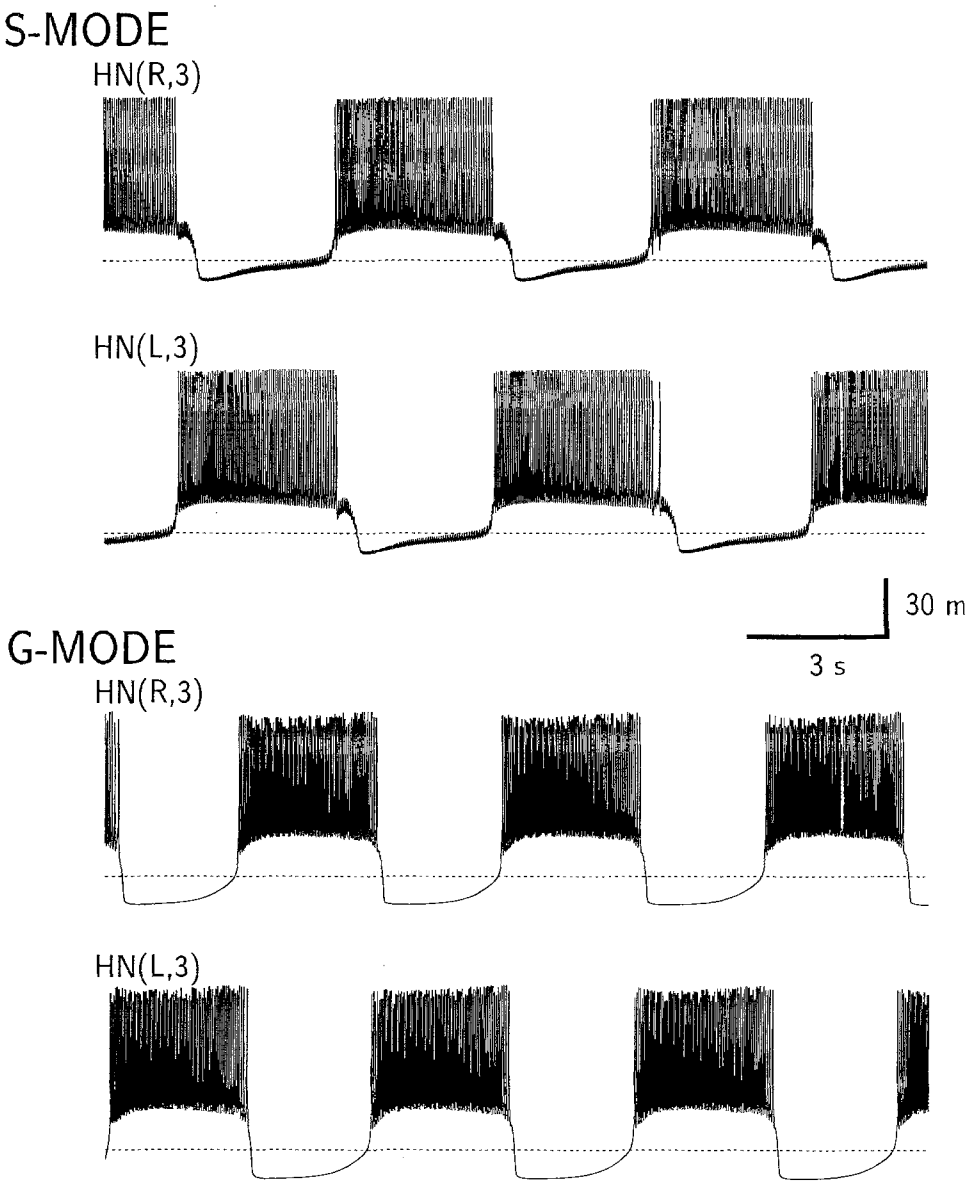

Fig. 10. Oscillations is S-mode and G-mode. Oscillations in G-mode are produced here by setting $\bar{g}_{\mathrm{SynS}} = 0$ and oscillations in S-mode are the "canonical" oscillations shown in Figs. 3 and 4. The amplitude of the underlying slow wave was larger in G-mode and the oscillations were faster. During the inhibited phase of G-mode oscillations, the membrane potential approached values very close to E_{Syn} (−62.5 mV). In contrast, the inhibited phase in S-mode was less inhibitory (the membrane potential never went below −59 mV), as can be seen by the spike-mediated IPSPs during that phase.

addition of the persistent Na^+ current I_P (Opdyke and Calabrese, 1994) and the spike-mediated synaptic current I_{SynS} (Simon et al., 1994). Other changes include modifying the inactivation and deactivation time constants of I_{CaS} and I_{CaF} as described in the methods section; slight modifications of I_h and I_{SynG} and tuning the maximal conductances of all ionic currents close to values measured experimentally. Adding I_P to the model enabled it to produce action potentials when synaptic transmission was blocked. The explicit dependence of synaptic transmission was necessary to produce spike-mediated IPSPs because in the graded-transmission model action potentials do not elicit sufficient Ca^{++} currents to reproduce fast IPSPs. The enacted modifications enabled the model to produce the following responses:

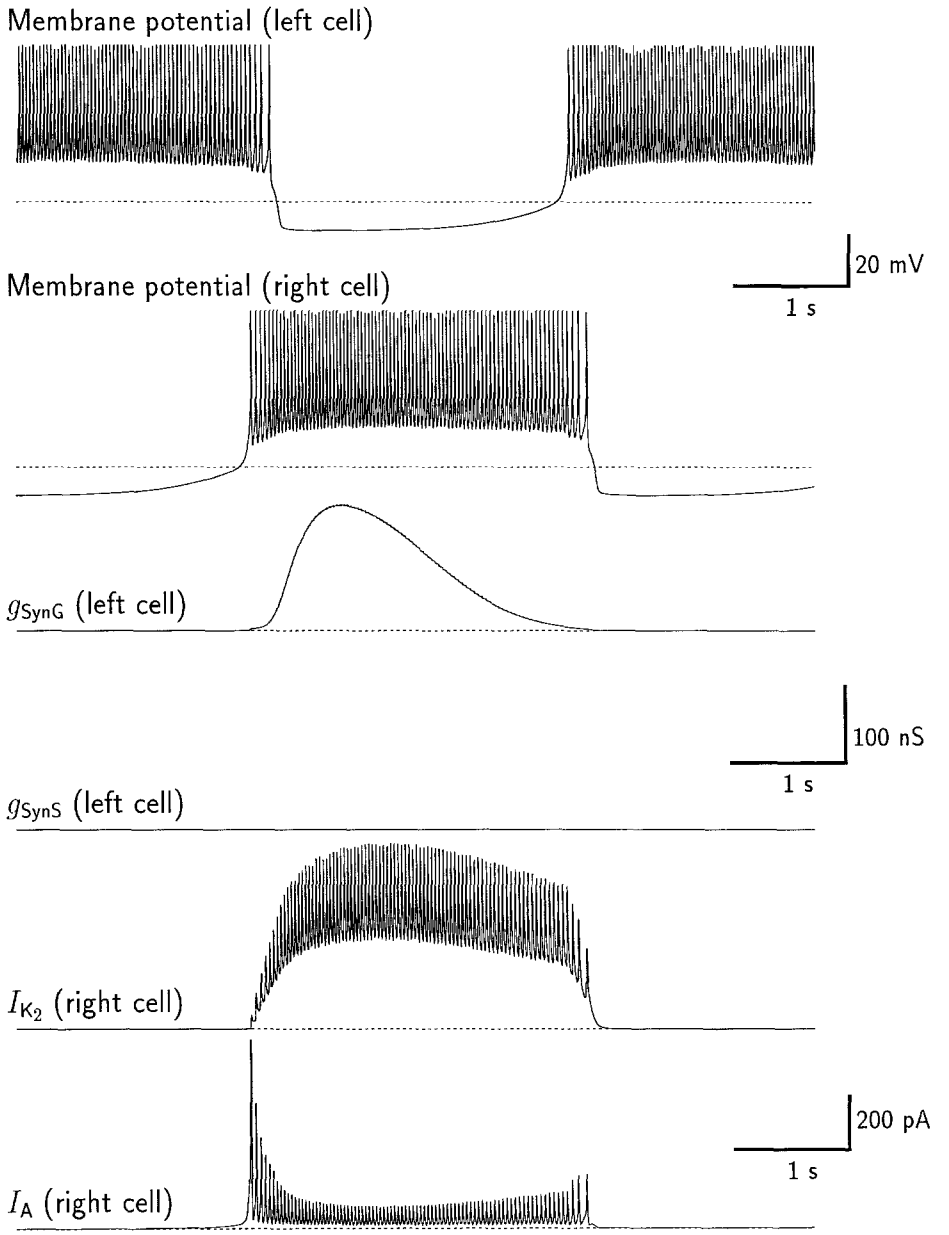

Fig. 11. One cycle of oscillations in the model cells in G-mode. Synaptic conductances and K^+ currents are shown on the same time scale. A comparison with Fig. 3 (S-mode) showed that g_{SynG} was active for the entire duration of the inhibited phase and was much larger in amplitude. The persistent K^+ current I_{K_2} was larger than I_{K_2} in S-mode because the amplitude of the plateaus was larger, but the transient current I_A was smaller.

The model cells produce bursting oscillations with a period of approximately 8 s, similar to the oscillations of the heart interneurons (period 8 to 12 s); both the model cells and the heart interneurons spike tonically when synaptic transmission is blocked. The model cells show passive properties similar to that of the heart interneurons in response to a hyperpolarizing step when synaptic transmission and I_h are blocked. Both the model cells and the heart interneurons are capable of producing slow oscillations when the external Na^+ concentration is reduced. In response to a hyperpolarizing current step injected in one cell, the model responds as the heart interneurons do: there is a hyperpolarization in the perturbed cell followed by

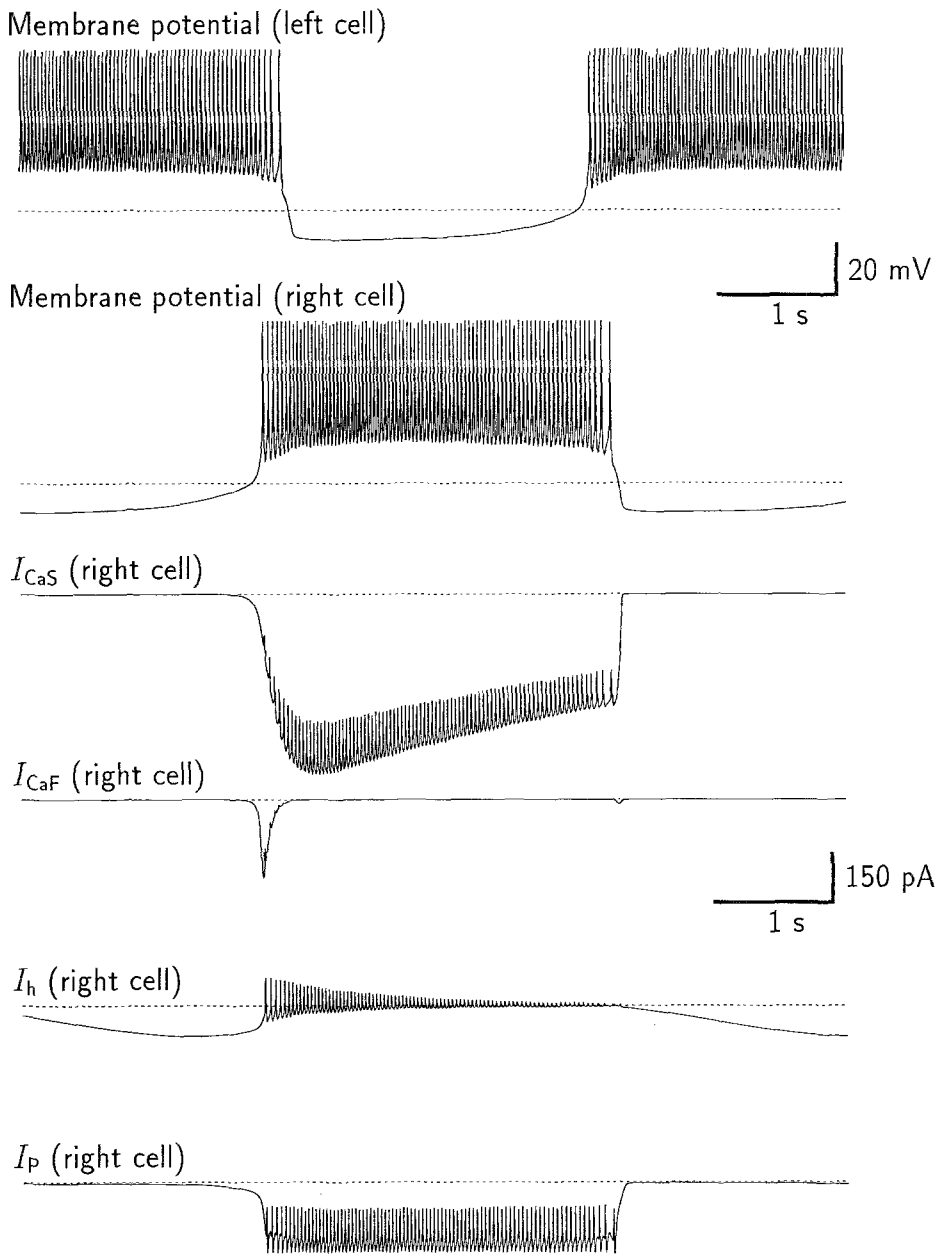

Fig. 12. One cycle of oscillations in the model cells in G-mode. Inward current are shown on the same time scale. As in S-mode oscillations (Fig. 4) I_{CaS} and I_P supported the plateau. The large graded IPSP in G-mode caused the cells to hyperpolarize to potentials near E_{Syn}. There was more removal of inactivation from the Ca^{++} currents compared to S-mode oscillations, resulting in larger currents and bigger plateaus. There was also more activation of I_h, which helped depolarize the cell during the inhibited phase and decreased the period of oscillations.

a depolarizing sag in the membrane potential and a large plateau-like depolarization on termination of the step; the opposite cell continues to fire during the step and, on termination of the step, is inhibited by a strong graded IPSP. The phase of the oscillations is reset when the step is terminated.

We have shown that two modes of oscillations can arise in the model cells: one dominated by spike-mediated synaptic inhibition (S-mode) and the other dominated by graded synaptic inhibition (G-mode). S-mode oscillations appear to be closer to the oscillation of the heart interneurons for several reasons:

1. Spike-mediated IPSPs of moderate size (3 to 5 mV) can be observed throughout the inhibited phase of the heart interneurons (Fig. 1), indicating that the membrane potential is not at E_{Syn}.
2. Even though the cells could potentially produce large and prolonged plateaus, such as when a hyperpolarizing current pulse is injected into the cell body (Figs. 7 and 8), such large plateaus are not present during normal oscillations.
3. During the inhibited phase the approach to the threshold for transition is more gradual under normal conditions of oscillation than when the cells rely solely on graded synaptic transmission, as in the slow oscillations shown in Fig. 9.
4. When the heart interneurons use primarily graded transmission the oscillations are faster than under normal conditions (Fig. 9). This change in period is consistent with the shorter period of oscillations seen when the model cells are in G-mode and is the result of the decay of the graded IPSP.

The cells HN(3) and HN(4) have posterior-projecting axons that span several segmental ganglia along the ventral nerve cord and make synaptic connections with the HE cells in these ganglia. Since the activity of HN(3) and HN(4) cells is generated primarily in the ganglion containing the cell body (the ganglion of origin) (Peterson 1983a;b), spike-mediated transfer may be the primary mode of synaptic transfer used by these cells in ganglia other than the ganglion of origin. The analysis of oscillations of model cells in S-mode and G-mode suggests that in the ganglion of origin itself spike-mediated inhibition, and not graded inhibition, may be the dominant method of synaptic transfer. The sustained synaptic inhibition in S-mode is provided by spike-mediated synaptic transmission that, in the heartbeat elemental oscillators, are relatively constant. The graded component of synaptic transfer, which is large but transient, is responsible for terminating the burst phase in the opposite cell when the cell escapes its inhibited phase. The graded IPSP is also a potential source of providing corrective strong inhibition to the opposite cell if the oscillation is perturbed. We emphasize that the difference between S-mode and G-mode oscillations is a consequence of spike-mediated synaptic transfer and not of spiking, which is present in both modes. Even though the oscillations in the HN cells appear to be closer to the S-mode oscillations, the cells could potentially switch to G-mode oscillations if spike-mediated transmission is reduced, or action potentials are blocked, as in the case of slow oscillations. Having the potential for producing oscillations using either graded or spike-mediated synaptic inhibition may be important in other systems as well.

Although our model incorporates the diversity of intrinsic and synaptic currents and reproduces various behaviors of the heart interneurons, there are aspects of the model that do not conform to observation or are assumptions. The plateaus in the burst phase of the model oscillations and the abrupt transition from the inhibited phase to the burst phase are not observed in oscillations of the heart interneurons. The action potentials in the model cells are much larger and higher in frequency than in the real cells. Both I_P and I_h in the model are smaller than measured in the heart interneurons. Blocking I_h in the heart interneurons disrupts normal activity and causes the cells to fire tonically. In the canonical model setting $\bar{g}_h = 0$ does not disrupt the oscillations but considerably increases the period. The activation and deactivation time-constants of I_{K_2} are assumed to be slow. There is an overlap in the burst phase of the two heart interneurons that is much smaller in the model. The spike frequency during the burst phase of the model is significantly higher than the spike frequency of the real heart interneurons (see Results). Reducing the spike frequency in the model reduces effective spike-mediated inhibition in the opposite cell, switches the oscillation to G-mode and reduces the period of oscillation. Moreover, the decline in spike frequency (from 23 Hz to 15 Hz) seen during the burst in the model cells is not observed in the heart interneurons, suggesting that release mechanisms may be less important in the biological oscillations. Keeping the higher spike frequency in the model can be somewhat justified by the fact that, during the inhibited phase, the heart interneuron of the elemental oscillator receives spike-mediated IPSPs not only from its contralateral homologue, but also from the ipsilateral cells HN(1) and HN(2) (see Introduction), although these IPSPs are smaller in amplitude. The amplitude of the spikes is also larger in the model than in the records of the heart interneurons (Fig. 1). This is not a major flaw, since the amplitude of the spikes does not directly affect spike-mediated IPSPs in the model. The model cell consists of a single isopotential compartment that oversimplifies the geometry of the heart interneurons. Some shortcomings of the model elemental oscillator, including the large amplitude of spikes, may be resolved with further experiment and by building a compartmental model that spatially separates the spike-generation zone from the

compartments containing the slower currents, especially the low-threshold Ca^{++} currents.

The Role of Some Ionic Currents in the Model

Oscillations in the model cells arise through the interaction of synaptic and intrinsic ionic currents. The hyperpolarization caused by inhibitory synaptic currents results in the activation of I_h and removal of inactivation from low-threshold Ca^{++} currents. During the inhibited phase, I_h and the noninactivating inward current I_P, which has low activation threshold, depolarize the membrane potential to the bursting threshold. The inward currents I_P and I_{CaS} then maintain the cells above threshold for spiking for the duration of that phase. The outward current I_{K_2}, which has a higher threshold and slower activation rate than the regenerative inward currents, but is also non-inactivating, balances the inward currents during the burst and prevents the cells from becoming too depolarized to produce action potentials. Since I_{K_2} affects the plateau potential of the slow wave underlying the burst phase, it also affects spike frequency and therefore spike-mediated transmission and the period of oscillations. The activation rate of I_{K_2} (≈ 100 ms) is much slower than the activation rate of I_{K_1} (2 to 10 ms). Therefore I_{K_2} cannot react fast enough during a spike to counteract I_{Na} and the falling phase of the action potentials is mainly supported by I_{K_1}. If I_{K_1} is removed from the model, even though slow wave oscillations persist, there are only a few spikes in the initial phase of the bursting plateau before inactivation of I_{Na} causes cessation of spiking. The membrane potential of the plateau in this case is around -20 mV, much higher than the undershoot of the action potentials in the canonical oscillations (-40 to -37.5 mV). Therefore, by activating the fast outward current I_{K_1}, action potentials control the height of the plateau during the oscillations. The effect of the outward currents on the polarization of the burst phase and spike frequency is significant in light of the fact that the activation and inactivation of outward currents is influenced by FMRF-NH_2, a known modulator of the heartbeat rhythm (Simon, Opdyke and Calabrese, 1992). We are in the process of studying these effects in the model.

The extent of removal of inactivation from the low-threshold Ca^{++} currents during the inhibited phase determines how large the graded IPSP produced during the next cycle will be. Since the Ca^{++} currents also inactivate at relatively negative potentials, the relationship between the inhibitory synaptic currents and the removal of inactivation from I_{CaF} and I_{CaS} is not a simple one. During the inhibited phase of oscillations, the time that the membrane potential of the cell is between -55 and -45 mV causes inactivation of the low-threshold Ca^{++} currents. Thus, by delaying the rise of the membrane potential during the inhibited phase, spike-mediated IPSPs can reduce the size of these Ca^{++} currents and therefore the amplitude of the graded IPSP.

We have described the properties of the heart interneurons that the model cells simulate. The fundamental processes that give rise to oscillations in the model cells appear to be close to those described for the heart interneurons (Calabrese, Angstadt and Arbas, 1989). During the inhibited phase of oscillations, the heart interneurons hyperpolarize to -60 to -50 mV, the range of potentials in which I_h is partially activated and there is removal of inactivation from I_{CaS} and I_{CaF}. Furthermore, there is evidence that I_P is activated when synaptic transmission is blocked and the cells spike tonically (see the results section). The extent to which spike-mediated or graded transmission is dominant during the oscillations of the heart interneurons is not known. We are currently conducting experiments to test whether graded synaptic transmission is transient during the inhibited phase of oscillations in the heart interneurons.

Two distinct mechanisms for oscillation of reciprocally inhibitory pairs of neurons, "escape" and "release," have been described by Wang and Rinzel (1992). In the escape mode, intrinsic mechanisms of the inhibited neuron overcome synaptic inhibition by its partner, and the neuron escapes to the active phase. In the release mode, the active neuron falls below the threshold of synaptic transmission, and its partner is released from inhibition. The bursting mechanism in our model contains elements of both escape and release modes. The escape mode is promoted by I_h, which is activated in the inhibited phase, and by I_P, which has a low activation threshold. The release mode is promoted by the decay of the synaptic currents; the graded component decays in amplitude and the spike-mediated component decays in frequency. The postsynaptic cell escapes from its inhibitory phase and begins spiking when the regenerative inward currents, with the help of I_h and I_l, overcome the inhibitory synaptic currents. The activation of I_h at hyperpolarized potentials allows it to significantly affect the length of the inhibited phase and hence the period of oscillations (Olsen et al., 1995). The interaction between the low-threshold ionic currents and the synaptic currents determines whether the release or the escape aspect is dominant.

Analysis of the intrinsic and synaptic currents in the model cells has enabled us to understand possible roles of the multiple currents in the heart interneurons. The interaction of ionic currents in the model can be explored by varying the maximal conductances of each current and studying the effect on the period of oscillations, the burst duration, spike frequency, and mode of oscillation. These interactions are difficult to study directly in the heart interneurons. In Olsen et al. (1995) we analyze in detail the effect of varying intrinsic and synaptic currents in the model. In particular, we are interested in defining more closely the parameter range that approximates the oscillations of the heart interneurons and discovering possible mechanisms for the modulation of these oscillations.

Acknowledgments

This work was supported by National Institute of Neurological Disorders and Stroke Grant NS-24072 to R.L. Calabrese.

Appendix

The membrane potential V of each cell in the model is given by the equation

$$-C\frac{dV}{dt} = \left(\sum_{\text{ion}} I_{\text{ion}}\right) + I_{\text{SynG}} + I_{\text{SynS}}$$

The value chosen for the membrane capacitance of the cell is $C = 500$ pF. The ionic currents I_{ion} are given by the Hodgkin-Huxley rate equations

$$I_{\text{ion}} = \bar{g}_{\text{ion}} m^p h^q (V - E_{\text{ion}})$$
$$\frac{dm}{dt} = \alpha_m(V)(1 - m) - \beta_m(V)m$$
$$\frac{dh}{dt} = \alpha_h(V)(1 - h) - \beta_h(V)h$$

Table 1 shows the rate constants (α or β) given by the function

$$\frac{c_1 + c_2 V + c_3 \exp\left(\frac{c_4+V}{c_5}\right)}{c_6 + \exp\left(\frac{c_4+V}{c_7}\right)}$$

Table 1. The rate parameters for the ionic currents.

Current	$\bar{g}_{\text{ion}}$(nS)	E_{ion}(mV)	g	State	Rate	c_1	c_2	c_3	c_4	c_5	c_6	c_7
I_{CaF}	16	135.2	$\bar{g}m^2h$	m	α	0.092	0	0	42		1	−2.8
					β	0.423	0.009	0	47		−1	1.7
				h	α	0.0027	0	0	51.5		1	2.7
					β	0.0165	0	0	49		1	−3.5
I_{CaS}	5	135.2	$\bar{g}m^2h$	m	α	0.0072	0	0	52		1	−3.5
					β	0.19	0	0	57		1	2.75
				h	α	0.00475	0	0	56		1	2.4
					β	0.00215	0.00003	0.0002	45.5	2.17		2.15
I_{P}	3	45	$\bar{g}m$	m	α	0.1	0	0	40		1	−5
					β	0.1	0	0	40		1	5
I_{Na}	350	45	$\bar{g}m^3h$	m	α	−47.25	−3.5	0	13.5		−1	−5
					β	7	0	0	11.5		1	6
				h	α	0.1	0	0	27.5		1	2
					β	0.255	0	0	12.5		1	−5
I_{K_1}	100	−80	$\bar{g}m^2h$	m	α	1	0	0	−10		1	−7.7
					β	1	0	0	72		8.5	28.6
				h	α	0.002	0	0	19		1	9.1
					β	0.00144	0	0	24		1	−5
I_{K_2}	50	−80	$\bar{g}m^2h$	m	α	0.2	0	0	2		20	−5.9
					β	0.2	0	0	15		20	6.7
I_{A}	80	−80	$\bar{g}m^2h$	m	α	0.335	0	0	32.5		0.86	−7.7
					β	2.48	0	0	50		7.5	8.3
				h	α	0.03	0	0	50		1	4.2
					β	0.029	0	0	56		1	−5
I_h	7	−21	$\bar{g}m^2$	m	α	−0.00082	−0.00002	0	44.6		0.94	0.75
					β	0.00042	0	0	52.8		1	−5.22
I_l	10	−52.5										
I_{SynG}	300	−62.5										
I_{SynS}	40	−62.5										

The graded synaptic current is

$$I_{\mathrm{SynG}} = \bar{g}_{\mathrm{SynG}} \frac{[\mathrm{P}]^3}{C + [\mathrm{P}]^3} (V - E_{\mathrm{Syn}})$$

$$\frac{d[\mathrm{P}]}{dt} = I_{\mathrm{Ca}} - B(V)[\mathrm{P}] \quad (I \text{ in nA})$$

$$I_{\mathrm{Ca}} = \max(0, -I_{\mathrm{CaF}} - I_{\mathrm{CaS}} - A)$$

where $C = 10^5$,

$$B(V) = 0.003 + 0.017/(1 + \exp(0.21(V + 43.6)))$$

and A is given by

$$\tau_A(V) \frac{dA}{dt} = A_\infty(V) - A$$

with

$$\tau_A(V) = 1000/(1 + \exp(0.3(V + 37)) + \exp(-(V + 45)))$$

$$A_\infty(V) = 0.1 + 0.2/(1 + \exp(-0.4(V + 37)))$$

The factors A, B, and C were chosen by fitting the presynaptic Ca^{++} currents and the postsynaptic IPSCs in Fig. 3 of Angstadt and Calabrese (1991).

The spike-mediated synaptic current is given by

$$I_{\mathrm{SynS}} = \bar{g}_{\mathrm{SynS}}(1 - e^{-t/\tau_{\mathrm{rise}}})e^{-t/\tau_{\mathrm{fall}}}(V - E_{\mathrm{Syn}})$$

where $\tau_{\mathrm{rise}} = 2.5$ ms and $\tau_{\mathrm{fall}} = 11$ ms are, respectively, the rising and falling time constant of the spike-mediated postsynaptic current.

Notes

The Neurolab modeling software and the HN model equations can be obtained on the World Wide Web at http://calabreselx.biology.emory.edu/.

References

Angstadt JD, Calabrese RL (1989) A hyperpolarization-activated inward current in heart interneurons of the medicinal leech. *J. Neurosci.* 9:2846–2857.

Angstadt JD, Calabrese RL (1991) Calcium currents and graded synaptic transmission between heart interneurons of the leech. *J. Neurosci.* 11:746–759.

Arbas EA, Calabrese RL (1987) Slow oscillations of membrane potential in interneurons that control heartbeat in the medicinal leech. *J. Neurosci.* 7:3953–3960.

Arshavsky YI, Orlovsky GN, Panchin YV, Roberts A, Soffe SR (1993) Neuronal control of swimming locomotion: Analysis of the pteropod mollusc *Clione* and embryos of the amphibian. *Xenopus*, *TINS* 16:227.

Beeler GW, Reuter H (1977) Reconstruction of the action potential of ventricular myocardial fibers. *J. Physiol. London* 268: 177–210.

Calabrese RL, Angstadt JD, Arbas EA (1989) A neural oscillator based on reciprocal inhibition, In: TJ Carew, D Kelley, eds. Perspectives in Neural Systems and Behavior, Alan R. Liss, New York. pp. 33–50.

Calabrese RL, De Schutter E (1992) Motor-pattern-generating networks in invertebrates: Modeling our way toward understanding: *TINS* 15:439–445.

Calabrese RL, Peterson EL (1983) Neural control of heartbeat in the leech, Hirudo medicinalis. In: A Roberts, B Roberts, eds. Neural Origin of Rhythmic Movements *Symp. Soc. Exp. Biol.* 37:195–221.

Connor JA, Stevens CF (1971) Inward and delayed outward membrane currents in isolated neural somata under voltage clamp. *J. Physiol. London* 213:1–19.

De Schutter E (1986) Alternative equations for the molluscan ion currents described by Connor and Stevens. *Brain Res.* 382: 134–138.

De Schutter E, Angstadt JD, Calabrese RL (1993) A model of graded synaptic transmission for use in dynamic network simulations. *J. Neurophysiol.* 69:1225–1235.

Friesen WO (1989) Neuronal control of leech swimming movements. In: JW Jacklet, ed. Neuronal and Cellular Oscillators, Marcel Dekker, Inc, New York and Basel.

Hodgkin AL, Huxley AF (1952) A quantitive description of membrane current and its application to conduction and excitation in nerve. *J. Physiol. London* 117:500–544.

Olsen ØH (1994) Exploring temporal computation in neuronal systems, University of Glasgow, PhD thesis, Department of Electronics and Electrical Engineering.

Olsen ØH, Nadim F, Calabrese RL (1995) Modeling the leech heartbeat elemental oscillator: II. Exploring the parameter space. *J. Comp. Neurosci.* 2:237–257.

Opdyke CA, Calabrese RL (1994) A persistent sodium current contributes to oscillatory activity in heart interneurons of the medicinal leech. *J. Comp. Physiol. A* 175:781–789.

Peterson EL (1983) Generation and coordination of heartbeat timing oscillation in the medicinal leech: II. Intersegmental coordination *J. Neurophysiol.* 49:626–638.

Peterson EL (1983) Generation and coordination of heartbeat timing oscillation in the medicinal leech: I. Oscillation in isolated ganglia. *J. Neurophysiol.* 49:611–626.

Satterlie RA (1985) Reciprocal inhibition and postinhibitory rebound produces reverbation in a locomotor pattern generator, *Science* 229:402–404.

Schmidt J, Calabrese RL (1992) Evidence that acetylcholine is an inhibitory transmitter of heart interneurons in the leech. *J. Exp. Biol.* 171:329–347.

Selverston AI, Moulins M (1985) Oscillatory neural networks. *Ann. Rev. Physiol.* 47:29–48.

Simon TW, Opdyke CA, Calabrese RL (1992) Modulatory effects of FMRF-NH_2 on outward currents and oscillatory activity in heart interneurons of the medicinal leech. *J. Neurosci.* 12: 525–537.

Simon TW, Schmidt J, Calabrese RL (1994) Modulation of high-threshold transmission between heart interneurons of the medicinal leech by FMRF-NH_2. *J. Neurophysiol.* 71:454–466.

Wang X-J, Rinzel J (1992) Alternating and synchronous rhythms in reciprocally inhibitory model neurons. *Neural Comp.* 4:84–97.